Muon-spin-relaxation studies of flux pinning in $Bi_2Sr_2CaCu_2O_8$ and $Pb_{0.7}Bi_{1.3}Sr_2CaCu_2O_8$

W. D. Wu, A. Keren, L. P. Le, B. J. Sternlieb, G. M. Luke, and Y. J. Uemura
Department of Physics, Columbia University, New York, New York 10027

P. Dosanjh and T. M. Riseman
Department of Physics, University of British Columbia, Vancouver, Canada V6T 2A3

(Received 29 May 1992; revised manuscript received 2 December 1992)

We have studied flux-depinning phenomena in the $Bi_2Sr_2CaCu_2O_8$ (Bi 2:2:1:2) and Pb-doped $Pb_{0.7}Bi_{1.3}Sr_2CaCu_2O_8$ (Pb-Bi 2:2:1:2) systems using the transverse-field muon-spin-relaxation (μSR) technique. Comparison of field-cooled (FC) and zero-field-cooled (ZFC) results with external fields applied along the c axis of single-crystal specimens defines an irreversibility temperature (depinning temperature) T_{irr}: the FC and ZFC relaxation rates are essentially identical above T_{irr}, while the relaxation rate in the ZFC measurements is larger than that in the FC measurements below T_{irr}, reflecting the increased inhomogeneity of the local fields in the ZFC measurements due to flux pinning. The irreversibility line $T_{irr}(H)$ in the H-T phase diagram for Bi 2:2:1:2, obtained by μSR measurements for several fields, is compared with previous results from ac-susceptibility and mechanical-oscillator measurements. Using a superconducting-quantum-interference-device (SQUID) magnetometer, the time-dependent diamagnetic magnetization has been measured in the same Bi 2:2:1:2 crystals. We show that the results from μSR and these other techniques can be explained consistently within a framework of the flux-creep model. The irreversibility temperature in Pb-Bi 2:2:1:2, determined by μSR measurements, is significantly higher than that in the pure Bi 2:2:1:2 system. This result, together with the larger critical current and the higher activation energy U_0 in the Pb-Bi 2:2:1:2 crystals as found by the SQUID magnetization measurements, suggests an enhancement of flux pinning by the Pb doping. We also compare the μSR results in sintered ceramic, oriented film, and single-crystal specimens in the pure Bi 2:2:1:2 system, and discuss possible effects of sample morphology on μSR measurements.

I. INTRODUCTION

Most type-II superconductors, including cuprate high-temperature superconductors (HTSC), exhibit irreversible magnetic phenomena:[1] the field-cooled (FC) magnetization is less diamagnetic than the zero-field-cooled (ZFC) magnetization below an irreversibility temperature T_{irr}. In most conventional superconductors, T_{irr} is very close to the superconducting transition temperature T_c. In some HTSC systems, however, the irreversibility temperature T_{irr} is considerably lower than T_c due to the high transition temperatures and usually small pinning energies, related to the short coherence lengths ξ. The field-temperature (H-T) phase diagram is divided into two large regions of reversible and irreversible behavior. It is generally believed that the irreversible regime is characterized by the pinning of magnetic flux vortices. At finite temperatures, thermal fluctuations cause dynamic motion of flux vortices, as indicated by the logarithmic time dependence of the diamagnetic magnetization. The flux-creep model[2] explain the separation of reversible and irreversible regimes as a result of a rapid change of the time scale of thermally activated flux motion around T_{irr}; this model does not involve a phase transition. In contrast, alternative models, such as flux melting or vortex glass models,[3] assume a phase transition of the flux lattice at T_{irr}. In spite of great experimental and theoretical effort, a detailed understanding of the thermal behavior of flux vortices does not exist. In order to study dynamic behavior, it is very useful to perform measurements of time- and temperature-dependent properties using methods having various time windows sensitive to different aspects of flux motion.

Palstra *et al.*[4] have demonstrated the thermally activated nature of the flux-creep process via resistance measurements of single crystal $Bi_{2.2}Sr_2Ca_{0.8}Cu_2O_{8+\delta}$. The resistance was found to be current independent and could be described by the Arrhenius law $\rho=\rho_0\exp(-U_0/kT)$, where the prefactor ρ_0 is independent of temperature, magnetic field, and orientation. The activation energy U_0 depends on the magnetic field, ranging from 0.03 to 0.3 eV near T_c. Mechanical oscillator measurements performed by Gammel *et al.*[5] give the field-dependent depinning temperature $T_{irr}(H)$ in the $Bi_2Sr_2CaCu_2O_8$ system at a frequency of 2 kHz. For a field of several teslas, T_{irr} was found to be about $\frac{1}{3}$ of the superconducting transition temperature $T_c\sim 80$ K. These two experiments, and other critical current measurements[6] in $Bi_2Sr_2CaCu_2O_8$ (denoted as Bi 2:2:1:2 henceforth) systems suggest that the magnetic flux vortices in this system are highly mobile over a broad temperature region above T_{irr}. Therefore, the 2:2:1:2 system is very suitable for studying flux depinning or flux melting phenomena.

Muon-spin relaxation (μSR) is a very powerful method in the study of local magnetic fields and their distribution.[7] In type-II superconductors at intermediate fields ($H_{c1}<H_{ext}<H_{c2}$), there is an inhomogeneous distribution of local fields due to the lattice of flux vortices. Thanks to this feature, one can deduce the magnetic-field penetration depth λ from the muon-spin-relaxation rate

σ, as demonstrated in extensive μSR measurements in high-T_c superconductors.[8] In this paper, we report μSR measurements in pure and Pb-substituted Bi 2:2:1:2 systems. Our results cover two different interests: methodological aspects of μSR studies of flux pinning and material research using μSR.

We first demonstrate how μSR detects flux depinning phenomena through the comparison of ZFC and FC measurements. This feature of μSR has been reported by Pümpin *et al.*[9] in their measurements of $YBa_2Cu_3O_7$ as well as by our prior conference report of a part of the present study in Bi 2:2:1:2,[10] and recently by Zimmermann *et al.*[11] in their interesting μSR measurements of current-induced flux motion. The present report involves the study of the magnetic-field dependence of the depinning temperature $T_{irr}(H)$ and the comparison with results obtained by the mechanical oscillator[5] and ac-susceptibility measurements.[31] We also present the results of a superconducting-quantum-interference-device (SQUID) magnetometer measurements of time-dependent diamagnetic magnetization in the same single crystals used in the μSR measurements. Within a framework of the flux-creep model, we construct a simple picture to explain the results from these different techniques consistently, and estimate a time window for the μSR technique in the study of flux-pinning phenomena.

Additionally, we report μSR measurements in Pb-substituted $Pb_{0.7}Bi_{1.3}Sr_2CaCu_2O_8$ single crystals (denoted as Pb-Bi 2:2:1:2 henceforth). In general, the critical current density in a superconductor is determined by the balance of the pinning and Lorentz forces on flux vortices. The introduction of defects into the crystal lattice, for example, by neutron[12,22] and ion irradiation,[13] shock compression,[14] or precipitation,[15] has often resulted in increased number of such pinning centers and correspondingly larger critical currents. Wang *et al.*[16] have reported that the critical current of Bi 2:2:1:2 system increases by an order of magnitude through the introduction of Pb in the system. It is then interesting to see if the flux depinning temperature T_{irr} is increased in Pb-substituted specimens.

Finally, we compare μSR measurements of Bi 2:2:1:2 using ceramic, thick-film, and single-crystal specimens, and discuss the dependence of the results on material morphology. In contrast to many other cuprate systems, such as $YBa_2Cu_3O_y$, the muon-spin-relaxation rate at low temperatures $\sigma(T\rightarrow 0)$ in Bi 2:2:1:2 depends strongly on the specimen morphology. Since a complete understanding of this phenomenon is not yet established, we will describe a few different possible interpretations, and discuss their consistency with the present results from μSR and SQUID measurements.

We begin by describing the procedure for sample preparation and characterization using susceptibility and critical current measurements in Sec. II. Next, we outline the μSR technique and discuss the principles of μSR measurements of the magnetic-field penetration depth λ in Sec. III. The results of transverse-field and zero-field μSR measurements in Bi 2:2:1:2 and Pb-Bi 2:2:1:2 are presented in Sec. IV. In Sec. V, we compare our μSR results with irreversibility lines obtained from the mechanical oscillator and ac- and dc-susceptibility measurements in the H-T phase diagram. The results of time-dependent dc-magnetization measurements are presented in Sec. VI, where their relation with the μSR results will be discussed. Basic features of the results in Sec. V and Sec. VI will be explained by a simple flux-creep model. Section VII provides discussion, including the effects of sample morphology in μSR measurements, followed by a summary and the conclusions we may draw from the present study.

II. SAMPLE PREPARATION AND CHARACTERIZATION

We mainly report μSR measurements performed on single-crystal specimens of Bi 2:2:1:2 and Pb-Bi 2:2:1:2. Single crystals of $Pb_xBi_{2-x}Sr_2CaCu_2O_8$, with $x=0$ and 0.7, were grown from copper oxide–rich melts.[17] Briefly, a mixture of PbO, Bi_2O_3, $SrCO_3$, $CaCO_3$, and CuO powders was melted at 1253 K, held there for 10 h, cooled at 2 K/h to 1073 K, and then furnace cooled to room temperature. Single-crystal pieces were extracted by cleaving the crystals along their $\hat{a}$-$\hat{b}$ planes.

Several superconducting phases[18] exist in the Bi-Sr-Ca-Cu-O system; among them are the 80-K phase with a nominal stoichiometry of Bi:Sr:Ca:Cu equal to 2:2:1:2 and 110-K phase with a ratio 2:2:2:3. Low-field magnetic flux expulsion (Meissner) measurements in the pure Bi 2:2:1:2 ($V=0.19\times0.13\times0.021$ cm^3, $m=2.2$ mg) and Pb-Bi 2:2:1:2 ($V=0.17\times0.11\times0.007$ cm^3, $m=0.55$ mg) single crystal were performed using a SQUID magnetometer. After a field of 20 Oe was applied perpendicular to the $\hat{a}$-$\hat{b}$ plane at 120 K, the magnetization was measured at each temperature down to 3 K (field-cooling measurements). Since it is always confusing how sample geometry and the size of the detecting coil affect the SQUID response, we discuss the measured magnetization M_{obs} and real magnetization M in the Appendix. The Appendix also shows that $M_{obs}=M$ holds for our measurements with an error less than 3%. The results shown in Fig. 1 exclude the significant existence of superconducting phases other than 2:2:1:2 phase. The superconducting transition temperature does not change much with the Pb doping, and a susceptibility $\chi'=-4\pi M/H_{ext}$ of 66% is obtained for both crystals. To estimate the Meissner fraction

$$\chi=-4\pi M/H=-4\pi(1-N)M/H_{ext}\ ,$$

we need to correct for the demagnetizing effect $1-N$. The demagnetizing factor N of both crystals is roughly estimated to be ~ 0.9 according to the "circular disk" approximation used in Ref. 19. This indicates that the Meissner fraction for both crystals is about $\sim 6\%$. It should be pointed out that the Meissner fraction obtained at $H_{ext}=20$ Oe does not represent superconducting volume fraction of the crystals, due to following arguments.

We know[19] that, when an external field $H_{ext}\leq(1-N)H_{c1}$ is applied to a type-II superconductor of arbitrary shape with a demagnetizing factor N, the superconductor is in the Meissner state and magnetic-field in-

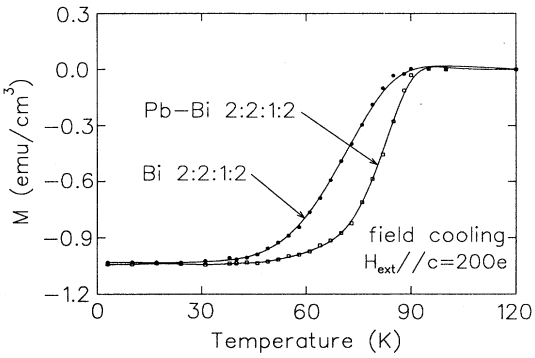

FIG. 1. dc-susceptibility measurements of Bi 2:2:1:2 and Pb-Bi 2:2:1:2 crystals in an applied field of 20 Oe. The results exclude the significant existence of superconducting phases other than 2:2:1:2 phase. The superconducting transition temperature does not change much with the Pb doping. The low-temperature Meissner fraction $\chi=4\pi(1-N)M/H_{\rm ext}$ for both crystals is estimated to be about 6% at the applied field 20 Oe.

duction B inside the superconductor equals zero,

$$B=H+4\pi M=H_{\rm ext}+4\pi(1-N)M=0\ . \tag{1}$$

The ideal Meissner fraction $\chi=-4\pi(1-N)M/H_{\rm ext}$ is equal to 1. The measured Meissner fraction χ can therefore be regarded as the superconducting volume fraction. If $H_{\rm ext}\geq(1-N)H_{c1}$, the superconductor is in the intermediate state and magnetic flux lines penetrate into the superconductor. The ideal Meissner fraction becomes smaller than 1, and the measured Meissner fraction can no longer be regarded as the superconducting volume fraction. Since reported values of H_{c1} of high-T_c materials are widely scattered,[1] and H_{c1} has not been determined for our crystals, it is not known whether the crystals are in the Meissner or intermediate state at the applied field $H_{\rm ext}=20$ Oe. Therefore, the measured Meissner fraction $\sim 6\%$ does not represent the superconducting volume fraction of the crystals.

We also note that for high-T_c materials, a low Meissner fraction is not surprising at a field of about 20 Oe. In Ref. 20, Krusin-Elbaum *et al.* reported that the Meissner fraction of the $YBa_2Cu_3O_2$ crystal decreases with increasing field, from $\sim 60\%$ at 0.1 Oe to $\sim 10\%$ at 20 Oe. This shows that, in order to measure the superconducting volume fraction, it is necessary to apply an external field as small as ~ 0.1 Oe (or less). Unfortunately, it was impossible to operate our SQUID magnetometer with $H_{\rm ext}\leq 20$ Oe.

The critical state model (or "Bean model") allows us to determine critical current J_c in these crystals from measurements of magnetization hysteresis. In the model, Bean[21] made a simple assumption that J_c is independent of B. In spite of this simplification, this model should allow comparison of relative J_c values between similar samples. Typical hysteresis loops measured with the applied magnetic field parallel to the $\hat{c}$ axis in the Bi 2:2:1:2 and Pb-Bi 2:2:1:2 crystals are shown in Fig. 2(a). The magnetization M was measured at 5 K with discrete values of the applied field. We see that the magnetization loop for the Pb-Bi 2:2:1:2 crystals exhibits significantly greater hysteresis than the pure Bi 2:2:1:2 crystals. Similar results have been previously reported by Wang *et al.*[16] When an infinitely long, rectangular sample of width f and length g ($f<g$) is placed in an external magnetic field $H\gg H_{c1}$, the critical current given by the Bean model is

$$J_c=\frac{20\Delta M}{f(1-f/3g)}\ , \tag{2}$$

where ΔM is the magnetization difference of the two hysteresis branches at same field.[22] Figure 2(b) shows the critical current J_c of the Bi 2:2:1:2 crystal obtained with Eq. (2) [see the Appendix for the validity of Eq. (2) in measurements of thin-plate specimens]. It is quite difficult to estimate the critical current J_c accurately in a specimen with a shape where the demagnetizing effect is important. Nevertheless, the critical currents at $H_{\rm ext}=0$ in the pure and Pb-doped crystals can be compared with each other within the framework of Bean model. For an infinitely long cylinder of radius R, it has been found that $4\pi|M|=B=H^*/3=2\pi J_cR/15$ at $H_{\rm ext}=0$, where $H^*=2\pi J_cR/5$ is a scaling factor, and M and B both represent averaged values. M is positive when the field is decreasing and negative when the field is increasing. For a specimen with a demagnetizing factor N, $H^*\propto J_c$ can be taken as a scaling factor; that is, $B/H^*=f(N,H_{\rm ext}/H^*)$, where $f(N,H_{\rm ext}/H^*)$ is a function de-

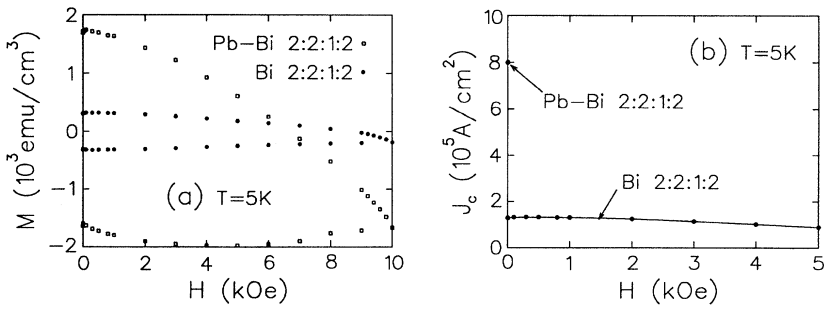

FIG. 2. (a) Magnetization loops of Bi 2:2:1:2 and Pb-Bi 2:2:1:2 crystals measured at 5 K using a SQUID magnetometer. The magnetization loop for the Pb-Bi 2:2:1:2 crystals exhibits significantly greater hysteresis than the Bi 2:2:1:2 crystals, implying enhanced flux pinning in the Pb-Bi 2:2:1:2 crystals. (b) Critical current J_c of the Bi 2:2:1:2 crystal calculated with Bean model. At $H_{\rm ext}=0$, we find that the critical current is increased by a factor of about 6 by the PB substitution.

pending on the sample geometry. At $H_{ext}=0$, we also have $B=H+4\pi M=4\pi(1-N)M$. Therefore, we know

$$M \propto B \propto H^* \propto J_c \quad \text{at } H_{ext}=0 , \tag{3}$$

where the coefficient is determined by the sample geometry. Since the Bi 2:2:1:2 and Pb-Bi 2:2:1:2 crystals have roughly same geometry, the ratio of critical current is roughly equal to the ratio of the magnetization M at $H_{ext}=0$. Figure 2(b) shows that the critical current, or equivalently the flux-pinning ability, is increased by a factor of about 6 by the Pb substitution at $H_{ext}=0$.

III. PRINCIPLES OF μSR EXPERIMENTS

Muon-spin relaxation (μSR) is an extremely sensitive method of measuring local magnetic fields in solids. Highly ($>95\%$) spin-polarized positive muons, with a range of about 140 mg/cm^2, are implanted one at a time in a target sample. After coming to rest at an interstitial site within $\sim 10^{-10}$ s, each muon precesses in the local magnetic field B_{loc} at a frequency $\omega=\gamma_\mu B_{loc}$, where $\gamma_\mu/2\pi=13.55$ MHz/kG. The local field is usually composed of a spatially constant contribution $\mathbf{B}_0$, due to a homogeneous applied field, and a spatially varying contribution, due to the nuclear magnetic moments or other magnetic mechanisms. Each muon decays into one positron and two neutrinos with a lifetime $\tau_\mu=2.2$ μs.

Once a muon is stopped in the sample, a clock in the data-acquisition system is started. The decay positron emitted from this muon is recorded by one of two counters (*EF* and *EB* or *EU* and *ED*), which are placed along and opposite to the initial muon-spin direction, as illustrated in Fig. 3. The detected positron produces a logic pulse to stop the clock, indicating the residence time t of the muon in the sample. Plotting positron event rate versus time t, we obtain a set of muon-lifetime histograms for each of the two counters. Since each positron

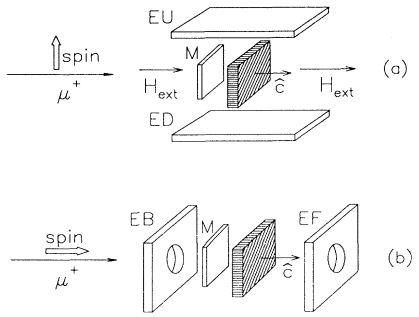

FIG. 3. (a) Schematic view of a typical TF μSR experimental arrangement. The incident muon beam, with its spin polarization perpendicular to the beam direction, is stopped in the specimen (shaded area). The incident μ^+ particle is identified by the counter M, and the time histograms of muon decay positrons are accumulated using counters *EU* and *ED*. The external field H_{ext} is applied perpendicular to the muon spin direction. (b) Schematic view of a typical experimental arrangement of ZF μSR. In the present work, the muon-spin polarization is along the beam direction (non-spin-rotated ZF μSR). In both TF μSR and ZF μSR geometries, the $\hat{c}$ axis of the single-crystal specimens was parallel to the beam direction.

is emitted preferentially along its parent muon-spin direction, the counting rates of the two counters N_+ and N_- exhibit an asymmetry, which reflects the muon-spin direction and polarization at time t. In terms of spin-polarization function $P(t)$ and time-independent normalization factors N_+ and N_-, and $N_+(t)$ and $N_-(t)$ can be written as

$$N_+(t)=N_+\exp(-t/\tau_\mu)[1+A_0P(t)] , \tag{4}$$

$$N_-(t)=N_-\exp(-t/\tau_\mu)[1-A_0P(t)] . \tag{5}$$

Typically more than 10^6 positrons are recorded in the histograms in each run. The asymmetry spectrum is defined as

$$A(t)=\frac{N_+(t)-\alpha N_-(t)}{N_+(t)+\alpha N_-(t)}=A_0P(t) , \tag{6}$$

$$\alpha=N_+/N_- , \tag{7}$$

where A_0, typically ~ 0.25, is the initial decay asymmetry, and α is determined by the experimental geometry.

The polarization function $P(t)$ is related to the probability distribution of magnetic fields $\rho(\mathbf{B})$ by

$$P(t)=\int\left[\frac{B_z^2}{B^2}+\frac{B_x^2+B_y^2}{B^2}\cos(\gamma_\mu BT)\right]\rho(\mathbf{B})d^3\mathbf{B} , \tag{8}$$

where the z axis is along the direction of initial muon polarization. The local magnetic-field distribution can thus be determined by measuring the time-dependent asymmetry spectrum. There are three kinds of μSR geometries: zero-field μSR (ZF μSR, with no magnetic field applied), transverse-field μSR (TF μSR, with a magnetic field applied perpendicular to the initial muon-spin direction), and longitudinal field μSR (LF μSR, with a magnetic field applied parallel to the initial muon-spin direction). Figure 3 shows a schematic view of the experimental configurations of the TF μSR and ZF μSR spectrometers used in the present experiments.

In TF μSR measurements, the polarization function $P(t)$ is given as a product of sinusoidal oscillation and a relaxation function $G_x(t)$,

$$P(t)=G_x(t)\cos(\omega t+\phi) . \tag{9}$$

If we assume a Gaussian distribution of magnetic fields $\rho(\mathbf{B})\propto\exp[-(B_x-B_0)^2/2(\Delta B)^2]$ of width $\Delta B=\sigma/\gamma_\mu$, the relaxation function takes a Gaussian form as

$$G_x(t)=\exp(-\tfrac{1}{2}\sigma^2t^2) , \tag{10}$$

and the frequency is given by $\omega=\gamma_\mu B_0$.

The magnetic-field penetration depth λ of type-II superconductors can be determined from the muon-spin-relaxation rate measured in TF μSR. When a type-II superconductor is placed in a homogeneous external magnetic field H_{ext} ($H_{c1}<H_{ext}<H_{c2}$), magnetic flux penetrates the specimen by forming a lattice of flux vortices. Usually, these vortices form a triangular lattice, called the Abrikosov lattice.[23] The distribution of local magnetic fields due to this flux lattice has been studied by Redfield[24] using nuclear magnetic resonance; the field distribution has a characteristic asymmetric shape. In actu-

al measurements, various averaging processes (angular averaging for ceramic specimens, effect of flux pinning, etc.) tend to make the field distribution closer to a Gaussian shape. Therefore, it is common to fit the μSR relaxation signal with a Gaussian envelope [Eq. (9)], and obtain the muon-spin-relaxation rate σ proportional to the width ΔB of this field distribution. Pincus *et al.* showed that this width ΔB is proportional to $1/\lambda^2$ and is nearly independent of the external field $H_{\rm ext}$ over a wide range of fields.

For an extreme type-II superconductor ($\kappa=\lambda/\xi \gg 1/\sqrt{2}$), the second moment of the local-field distribution

$$\sqrt{M_2}=\Delta B=\sqrt{\langle (B-\bar{B})^2\rangle}$$

has been shown to be

$$\sqrt{M_2}=\alpha\Phi_0/\lambda^2=\sigma/\gamma_\mu\ , \tag{11}$$

where $\Phi_0=2.70\times10^{-7}$ G cm^2 is the flux quanta, and the proportionality constant α depends on different models for the field distribution and functional forms of $G_{x(t)}$. After modifying the calculation of Pincus *et al.*[25] (performed for a square flux lattice) for a triangular lattice, one obtains $\alpha=0.0417$. A more rigorous calculation by Brandt[26] gives a larger value of $\alpha=0.0609$, since the "high-field tail" in the Abrikosov field distribution contributes heavily to M_2. When we fit $G(t)$ with a Gaussian function, however, the derived width does not reflect much of this high-field tail. We performed a simulation study assuming the Abrikosov distribution, fitted $G_x(t)$ with a Gaussian function, and obtained σ corresponding to $\sim 0.7\sqrt{M_2}\times\gamma_\mu$. Therefore, in our previous work, we used the conversion factor $\alpha=0.0417$ to deduce absolute values of the penetration depth λ as

$$\lambda=\frac{2700}{\sqrt{\sigma}} \tag{12}$$

with λ in Å and σ in μs^{-1}. In this paper, we are mostly concerned about the effect of flux pinning on σ. Hence, the choice of the value for α does not change the story of the present paper.

If the local magnetic fields fluctuate, or the implanted muons hop among lattice sites, then the muons see an averaged magnetic field. The distribution of local fields can be narrowed, resulting in a reduction of the relaxation rate. The effect of muon diffusion can be checked in zero-field μSR measurements, which are extremely sensitive even to very slow dynamical effects. In various cuprate HTSC systems, previous ZF μSR results[27] indicate that nuclear dipolar fields are static on a time scale of more than 1 μs below room temperature; there is no effect of muon diffusion. As shown in the next section, we confirmed this feature in the present Bi 2:2:1:2 system.

Motion of flux vortices could also result in dynamical narrowing of the field distribution. The distance between two adjacent vortices is $a=(\frac{4}{3})^{1/4}\sqrt{\Phi_0/B_0}$ for a triangular flux lattice. For fields of 1 ~ 15 kG used in the present study, a is in a range of 500–1500 Å, indicating that the field distribution varies on a quasimacroscopic length scale. Then, the narrowing can be expected only when flux vortices move more than distance a within a time scale of a microsecond. The feasibility of this effect in Bi 2:2:1:2 systems will be discussed in Sec. VII.

IV. μSR EXPERIMENTAL RESULTS

The experiments reported here were performed at the TRIUMF M15 surface muon channel. The specimens were mounted on a Fe_2O_3 sample holder in a ^{4}He gas flow cryostat with Mylar windows. Since muon spins depolarize very quickly in Fe_2O_3 below room temperature, the sample holder was made with this material to reduce background signals. Single-crystal specimens were mounted with their $\hat{c}$ axis parallel to the muon momentum, as shown in Fig. 3(a). Transverse fields were applied along the muon momentum, with the initial muon-spin polarization rotated perpendicular to the muon momentum. In the present study, all of samples were measured both by cooling through T_c in presence of an external field (FC) and by applying a field after cooling through T_c in zero external field (ZFC). To study the temperature dependence of ZFC results in an external field, we established a ZFC state at the lowest temperature and then raised the temperature. At several different temperatures, we confirmed that this process gives relaxation rates essentially identical to those in real ZFC procedures. In Fig. 4, we show several typical asymmetry spectra measured at 90 K FC, 10 K FC, and 12 K ZFC in the Bi 2:2:1:2 crystals. Because the raw asymmetry spectra oscillate very rapidly in the transverse fields we applied, the data are displayed in a rotating reference frame (RRF), with the refence frequency chosen to be close to

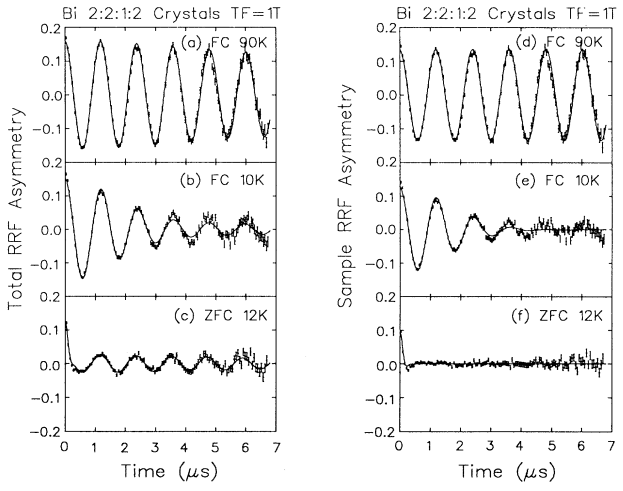

FIG. 4. (a)–(c) Typical asymmetry spectra $A(t)=A_s(t)+A_b(t)$ measured in Bi 2:2:1:2 crystals. Because the sample signal $A_s(t)$ decays to zero very rapidly at low temperatures in the ZFC measurements, the long-lived oscillating signal observed in (c) can be used to estimate the background signal $A_b(t)$. (d)–(f) Corresponding sample signals after the background signal is subtracted from the total signals. The relaxation rate increases below T_c in the FC measurements and becomes very large at low temperatures in the ZFC measurements. The solid lines in (d)–(f) are fits to Eq. (13).

the real frequency of oscillation ω.

To fit the observed asymmetry spectra, we used the sum of a sample signal $A_s(t)$ assuming a Gaussian distribution of magnetic fields inside the specimen and a background signal $A_b(t)$ produced by those muons stopped either in nonsuperconducting portions of the specimen or in the cryostat:

$$A_s(t)=A_s\exp(-\tfrac{1}{2}\sigma^2t^2)\cos(\omega t+\phi)\ , \tag{13}$$

$$A_b(t)=A_b\exp(-\tfrac{1}{2}\sigma_b^2t^2)\cos(\omega_b t+\phi)\ . \tag{14}$$

In Fig. 4(c), we see that the ZFC asymmetry spectrum at 12 K has a long-lived oscillating part. Because the sample signal following ZFC at low temperatures usually has a very large relaxation rate $\sigma\approx 10\ \mu s^{-1}$, $A_s(t)$ decays to zero very quickly. This allowed us to use the long-lived oscillating part to estimate the background signal $A_b(t)$. Assuming that the background signal does not depend on temperature, we subtracted $A_b(t)$ from the total asymmetry spectrum to obtain the sample asymmetry spectrum $A_s(t)$. The initial asymmetry A_b of the background signal corresponds to about 13% of the total asymmetry (A_s+A_b). Thanks to the small amount of background, different methods for background subtraction do not make a significant difference to the observed results.

The sample asymmetry spectra are shown in the right half of Fig. 4 [Figs. 4(d)–4(f)]. We see that the sample relaxation rate increases below T_c in the FC measurements. The significant difference between the FC and ZFC results is evident at low temperatures. Figure 5 shows the temperature dependence of the muon-spin-relaxation rate σ measured in single crystals of Bi 2:2:1:2 [Fig. 5(a)] and Pb-Bi 2:2:1:2 [Fig. 5(b)] at a few different external fields. Above T_c, the nonzero relaxation rate is due to inhomogeneous nuclear dipolar fields. In the FC measurements, the relaxation rate σ increases with decreasing temperature below T_c and shows saturation at low temperatures. This behavior has been observed in many other cuprate superconductors.[8,28] The increase of σ below T_c is due to decrease of the penetration depth λ with decreasing temperature in the superconducting state.

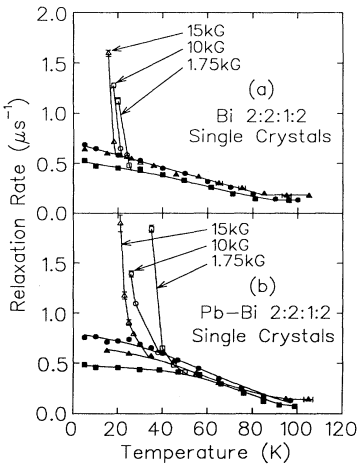

FIG. 5. Gaussian relaxation rates σ for (a) Bi 2:2:1:2 and (b) Pb-Bi 2:2:1:2 single crystals obtained in transverse-field measurements. The increase of σ below T_c is due to the decrease of the penetration depth λ with decreasing temperature in the superconducting state. At a given field, there exists a characteristic temperature (depinning temperature) T_{irr}, above which $\sigma_{ZFC}=\sigma_{FC}$, and below which $\sigma_{ZFC}>\sigma_{FC}$. The flux equilibrium state cannot be reached below T_{irr} in the ZFC procedures due to flux pinning, resulting in an enhanced inhomogeneity of local fields.

In the results for a given external field, there exists a characteristic temperature T_{irr}, above which $\sigma_{ZFC}=\sigma_{FC}$ and below which $\sigma_{ZFC}>\sigma_{FC}$. In the present measurements, we adopted an experimental configuration with the external field applied perpendicular to the plate-shaped specimens, where the demagnetizing factor is close to 1. In this geometry, the total magnetic flux in the specimen does not change much above and below T_c in the FC measurements. Therefore, the flux vortices do not have to move macroscopic distances to reach an equilibrium flux lattice configuration in the FC procedure. In contrast, when we establish the superconducting state and then apply an external field in the ZFC measurements, the flux vortices have to move distances of the order of a sample dimension before reaching the equilibrium state. If some flux vortices are pinned by trapping centers during this macroscopic motion, the vortex lattice cannot reach the equilibrium configuration. This leads to an increased inhomogeneity of the local-field distribution and a corresponding increase in σ. The difference between the relaxation rates in the FC and ZFC measurements below T_{irr} indicates that the flux vortices cannot reach the equilibrium state in the ZFC procedures below T_{irr}. In this way, flux-pinning-depinning phenomena can be studied by μSR.

Figure 5 shows the results in three transverse magnetic fields 1.75, 10, and 15 kG. The relaxation rate in FC measurements does not show much field dependence, as predicted by the calculations of Pincus[25] and Brandt.[26] Part of the small dependence on field may be due to the choice of background signal. We find, however, that the depinning temperature T_{irr} decreases with increasing external magnetic field. The irreversibility temperatures of Bi 2:2:1:2 and Pb-Bi 2:2:1:2 singly crystals are plotted in Fig. 6 as a function of H_{ext}. As we will discuss in the next section, the field dependence of the irreversibility temperature has also been studied by other experimental techniques. Figure 6 shows the irreversibility line in the H-T plane, which can be compared with various theories of flux depinning and/or melting.

To study the effect of Pb substitution in flux pinning, we performed μSR measurements in the pure Bi 2:2:1:2 and Pb-substituted Pb-Bi 2:2:1:2 using the same external fields. The FC relaxation rates of the Pb-Bi 2:2:1:2 crystals are very close to that of the pure Bi 2:2:1:2 crystals, indicating that the equilibrium configuration of local magnetic fields inside the pure Bi 2:2:1:2 crystal is essentially unchanged by the substitution of Pb. As in the case of the pure Bi 2:2:1:2 crystals, the depinning temperature in the Pb-Bi 2:2:1:2 crystals decreases with increasing external field. For a given external field, however, the depinning temperature is significantly higher in the Pb-Bi

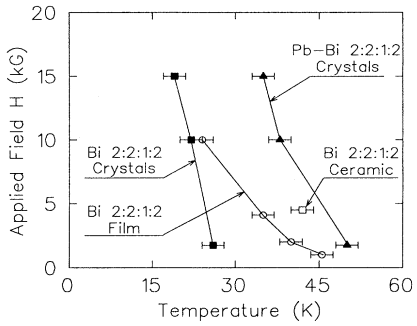

FIG. 6. Irreversibility lines of Bi 2:2:1:2 crystals (present study), thick film (Ref. 10), ceramic (Refs. 10 and 28), and Pb-Bi 2:2:1:2 crystals (present study). The depinning temperature T_{irr} in the Bi 2:2:1:2 crystals is increased substantially with the Pb substitution.

2:2:1:2 crystals relative to pure Bi 2:2:1:2 crystals, as shown in Figs. 5 and 6. This indicates that the chemical substitution of Pb strengthens flux pinning in the crystals. Such enhanced pinning could be due to increase of the number of the pinning sites and/or due to increase in the activation (trapping) energy. We will present magnetization measurements of the activation energy in Sec. VI, to further discuss this result.

In contrast to the $YBa_2Cu_3O_7$ system, μSR results in Bi 2:2:1:2 systems depend significantly on sample morphology. In Fig. 7, we compare the relaxation rate measured in the present single-crystal specimens with those obtained in sintered ceramic and thick-film specimens of Bi 2:2:1:2.[10,28] The low temperature relaxation rate $\sigma(T\rightarrow 0)$ in FC measurements for single crystals is less than half of the value for ceramic specimens. In Fig. 6, we show the irreversibility temperatures T_{irr} of the ceramic and film specimens of Bi 2:2:1:2 to compare with the results from single-crystal specimens in the present work. The irreversibility temperature T_{irr} tends to be lower for the crystal specimens compared to the ceramic or film specimens. To further study the effect of morphology, we crushed the single-crystal specimens of Bi 2:2:1:2 used in the present study, pressed the powder into a thin pellet, and then performed μSR measurements. As shown in Fig. 7, the low-temperature FC relaxation rate increases about 50% compared to the results for the same crystals before crushing. The origin of the dependence on sample morphology will be discussed in Sec. VII.

In μSR studies of the penetration depth λ, it is generally important to perform not only TF μSR but also ZF μSR measurements to confirm that there is no effect of magnetic order in the observed results. Figure 8(a) shows the zero-field-relaxation function $A_0G_z(t)$ observed in the single-crystal specimens of Bi 2:2:1:2 at a few different temperatures. Figure 8(b) shows the exponential relaxation rate σ_{exp} obtained by fitting the spectra to

$$A_0[\tfrac{1}{3}+\tfrac{2}{3}(1-\Delta^2t^2)\exp(-\tfrac{1}{2}\Delta^2t^2)]\exp(-\sigma_{exp}t)$$

with fixed $A_0=0.22$ and $\Delta=0.14\ \mu s^{-1}$. Above $T\sim 5$ K, we see the shape of $G_z(t)$ characteristic of static nuclear dipolar fields, and there is essentially no temperature dependence in the relaxation rate. This confirms the ab-

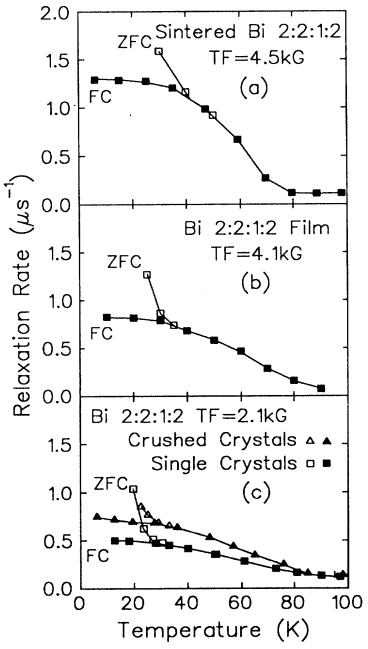

FIG. 7. Gaussian relaxation rates for Bi 2:2:1:2 single crystal, thick film (Ref. 10), and sintered ceramic (Refs. 10 and 28) specimens. The low-temperature FC relaxation rate $\sigma(T\rightarrow 0)$ in the single crystals is less than half of the value in the ceramic specimens.

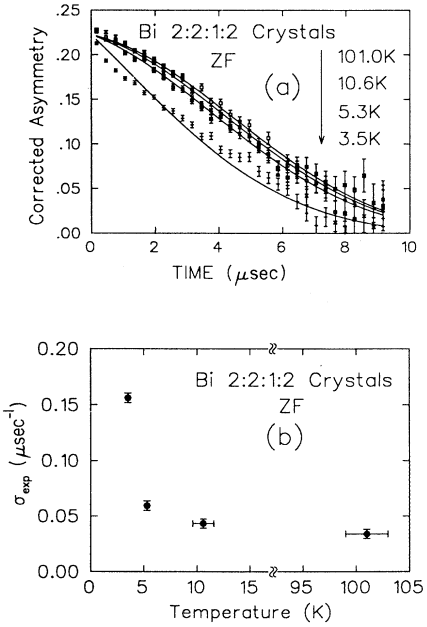

FIG. 8. (a) Zero-field relaxation function $A_0G_z(t)$ observed in Bi 2:2:1:2 single crystals. (b) Fitted exponential relaxation rate σ_{exp}. The increase of σ_{exp} below $T\sim 5$ K indicates onset of magnetic order in a portion of the specimen.

sence of muon diffusion in Bi 2:2:1:2 below 100 K. Below $T \sim 5$ K, the relaxation rate in zero field increases, indicating that a part of the specimen undergoes static magnetic order. Previous μSR studies in $Bi_2Sr_{3-x}Y_xCu_2O_8$ (Ref. 29) have shown that when the hole concentration is reduced in Bi 2:2:1:2, the superconducting temperature T_c decreases. With further reduction of the carrier density, magnetic order appears with disappearance of superconductivity. The present observation of magnetic order in a part of the specimens indicates a large distribution of carrier concentration within the present single-crystal specimens, which is due presumably to a macroscopic spatial inhomogeneity of oxygen concentration. From the present ZF μSR results, it is difficult to estimate the volume fraction of the "magnetic" part of the specimens. The ratio of initial asymmetry $A_s/(A_s+A_b)=87\%$, obtained in TF μSR, provides a lower limit of superconducting volume fraction. Therefore, in spite of the partial magnetic order, the major part of the present specimens can still be regarded as a "good" superconductor.

V. IRREVERSIBILITY LINES FORM DIFFERENT TECHNIQUES

The irreversibility lines in Fig. 6 exhibit a tendency for the depinning temperature to decrease with increasing external field. When a superconductor experiences a magnetic field stronger than H_{c1}, the arrangement of vortices is determined by competition between the pinning forces, the magnetic force that drives magnetic flux into the superconductor, and the thermal fluctuations of vortices. Above the depinning temperature T_{irr}, the magnetic driving force and/or the thermal fluctuations are strong enough to overcome the pinning potential. The response to thermal fluctuations can be studied using such dynamical probes as mechanical oscillator or ac-susceptibility measurements. In this section, by comparing T_{irr} estimated from different probes (with different time windows), we consider dynamical aspects of the depinning phenomena.

Using a mechanical torsion oscillator, Gammel *et al.*[5] measured the dissipation signal at a frequency $\omega_f=12.6$ kHz ($\nu=2$ kHz) as a function of temperature in several different external magnetic fields. One expects the maximum dissipation when the dynamic time scale of the flux motion matches the measuring frequency. They defined the temperature, which gives maximum dissipation as the melting (or depinning) temperature T_{irr}. Their results of T_{irr} in pure Bi 2:2:1:2 single crystal are shown in Fig. 9 in the H-T phase diagram. Ac-susceptibility measurements have been performed by Kes and Beck[31] in Bi 2:2:1:2 at the frequency of $\omega_f=550$ Hz ($\nu=87$ Hz); the results are also plotted in Fig. 9. Note that these results were obtained in specimens different from those in the present paper. In Fig. 9, we also included T_{irr} determined by the present μSR measurements, as well as the irreversibility temperature we obtained by dc-magnetization measurements using the same Bi 2:2:1:2 single crystals.

Dynamic motion of flux vortices creates dissipation and contributes to the electrical resistivity below T_c.

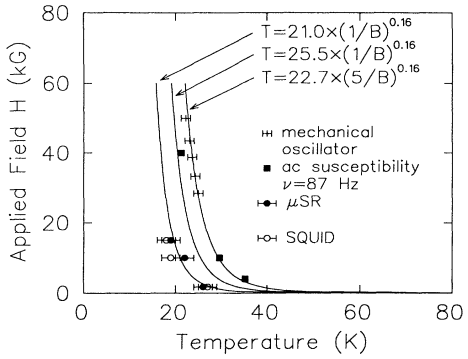

FIG. 9. Irreversibility lines of Bi 2:2:1:2 single crystals determined by mechanical oscillator (Ref. 5), ac-susceptibility (Ref. 31), μSR and dc-susceptibility (present study) measurements. Assuming the activation energy U_0 [Eq. (15)] estimated in the resistivity measurements (Ref. 4) and the vortex relaxation time $\tau(T,H)$ given by the flux-creep model [Eq. (16)], different irreversibility lines are expected for experiments having different characteristic frequencies ω_f [Eq. (17)]. The preexponential factor in Eq. (16) $\tau_0=1.1\times10^{13}$ s is determined by fitting the mechanical oscillator results to Eq. (17) (the furthest-right line). Using this τ_0 and $\omega_f=550$ Hz, an irreversibility line is obtained (the middle line) for the ac-susceptibility measurements. The best fit to the results obtained by μSR and dc-susceptibility measurements indicates these two measurements probe the depinning phenomena with much slower time scale (the left line represents $\omega_f=0.8$ Hz).

Palstra *et al.*[4] observed the thermally activated behavior of resistivity, and estimated the activation energy U_0, which was found to be essentially independent of temperature (i.e., the activated behavior is well followed over a wide temperature range). The field dependence of U_0 is given as

$$U_0(\mathbf{H}\|\hat{\mathbf{c}})=\begin{cases}600H^{-0.16} & \text{when } H<50 \text{ kOe}\\ 750H^{-0.33} & \text{when } H>50 \text{ kOe.}\end{cases} \quad (15)$$

Here, we demonstrate that the results in Fig. 9 can be explained consistently in the simple flux-creep model. In this model, the vortex relaxation time $\tau(T,H)$ is given as

$$\tau(T,H)=\tau_0\exp[U_0(H)/T] \ . \quad (16)$$

At the depinning temperature T_{irr} determined by a dynamic probe of characteristic frequency ω_f, we expect that the fluctuation time τ corresponds to $1/\omega_f$. The equation $\tau(T_{irr},H)=1/\omega_f$ gives us an expression for the irreversibility line

$$T_{irr}=-\frac{U_0(H)}{\ln(\omega_f\tau_0)} \ . \quad (17)$$

Assuming the activation energy $U_0(H)$ given in Eq. (15), and $\omega_f=12.6$ kHz, the results from mechanical oscillator measurements in Fig. 9 can be fit to Eq. (17). The further right solid line in Fig. 9 represents such a fit, which generally agrees well with the field dependence of T_{irr}, and yields a pre-exponential factor $\tau_0=1.1\times10^{-13}$ s. In this

way, the flux-creep model can explain the results of mechanical oscillator and resistivity measurements consistently.

Let us consider if this value of the pre-exponential factor τ_0 is reasonable. If we treat a vortex of length d as a quantum particle, the uncertainty principle can be used to estimate the vortex vibration frequency when the vortex is confined in a well of length x. The mass of the "particle" is $m = H^2\lambda_{ab}^2 d/8\pi c^2$. Here we use the in-plane penetration depth λ_{ab} rather than the coherence length ξ_{ab} because the motion of the vortex core results in motion of the whole magnetic field due to that vortex. The vibrating frequency given by the uncertainty principle $mvx \sim \hbar$ is

$$\nu \sim \frac{v}{x} \sim \frac{4hc^2}{H^2\lambda_{ab}^2 x^2 d} . \tag{18}$$

For typical values of $H = 10$ kOe, $\lambda_{ab} = 3\times10^{-5}$ cm, $x = \xi_{ab} = 2\times10^{-7}$ cm, and the superconducting plane spacing $d = 2\times10^{-7}$ cm, we obtain $\nu = 4\times10^{16}$ Hz. In this consideration, we have assumed that the vortex segment of length d moves independently without any correlation with segments between other superconducting planes. When the interlayer vortex correlation is considered, the oscillating frequency should be smaller than the above value. Using a typical thickness of single crystals $d = 2\times10^{-2}$ cm in Eq. (18), we have $\nu = 4\times10^{11}$ Hz, which corresponds to $\tau = 1/2\pi\nu = 4\times10^{-13}$ s. This argument confirms that the order of magnitude of the pre-exponential factor estimated from the mechanical oscillator measurements is reasonable.

Assuming $\tau_0 = 1.1\times10^{-13}$ s, we can draw an irreversibility line for ac-susceptibility measurements, substituting $\omega_f = 550$ Hz in Eq. (17). The middle solid line in Fig. 9 represents that line. The susceptibility results in high field agree relatively well with this line; at lower fields there is some inconsistency. The irreversibility points from μSR and dc-magnetization measurements agree well with each other. If we fit these points to Eq. (17), the best fit (the left solid line) is obtained for the measuring frequency corresponding to $\omega_f \sim 0.8$ Hz. This result indicates that these two measurements probe depinning phenomena with a much slower time scale. Further detailed arguments about the time window of μSR and magnetization studies will be given in the next section.

In Fig. 9, we see that the irreversibility lines determined by these different techniques can be explained fairly well by the flux-creep model, using the same pre-exponential factor τ_0 and the activation energy U_0 obtained form resistivity measurements. There is much debate concerning the nature of flux motion in HTSC. Of particular interest is whether the irreversibility line $T_{irr}(H)$ represents a phase transition of the flux-line system (e.g., melting of the crystalline flux lattice or of a disordered, glasslike flux lattice) or a temperature region where the flux creep is enhanced due to high operating temperatures. Here we have shown that the flux creep model works reasonably well. This, however, does not necessarily preclude or invalidate the "phase transition" scenarios.

VI. MEASUREMENTS OF TIME-DEPENDENT MAGNETIZATION

To obtain further detailed information on the dynamic behavior of flux vortices, we have performed dc-magnetization measurements of the Bi 2:2:1:2 and Pb-Bi 2:2:1:2 crystals used in our μSR studies, using a commercial SQUID magnetometer (Quantum Design MPMS). We measured the zero-field-cooling (ZFC) magnetization $M_{ZFC}(t)$ as a function of time t after a zero-field-cooling state was established, with the external field H_{ext} applied parallel to the $\hat{c}$ axis. Since a field-cooling (FC) state is an equilibrium state, the FC magnetization M_{FC} is independent of time t. After a field was applied above T_c, we measured M_{FC} at each temperature down to the lowest temperature. Above the irreversibility temperature T_{irr}, the FC magnetization M_{FC} and the ZFC magnetization $M_{ZFC}(t)$ are essentially identical. Below T_{irr}, the magnetization is history dependent with $|M_{ZFC}|$ larger than $|M_{FC}|$, since flux pinning prevents the vortices from quickly entering the specimens in the ZFC procedure, resulting in enhanced ZFC magnetization. Due to the thermally activated motion of flux vortices, the ZFC magnetization approaches the FC value slowly as a function of time, reflecting rearrangements of flux vortices towards the more equilibrated state achieved in the FC procedure. The time-dependent magnetization $M(t) \equiv |M_{ZFC}(t) - M_{FC}|$ thus reflects the dynamic motion of flux vortices.

Figure 10 shows the time dependence of $M(t)$ observed in Bi 2:2:1:2 crystals with $H_{ext} = 1.75$ kOe applied parallel to the $\hat{c}$ axis. We see that the irreversibility effect is more pronounced at lower temperatures, while $M(t)$ becomes smaller than the instrumental resolution (~ 0.1 emu/cm^3) above $T = 26$ K. Thus the irreversibility temperature $T_{irr} = 26$ K for $H_{ext} = 1.75$ kOe can be determined in this dc-magnetization measurement with a time window of $t \sim 10^2$ s. As shown in Fig. 10(c), the time dependence of $M(t)$ follows a logarithmic behavior over a wide range of temperature and time. The relative change of $M(t)$, normalized by $M(t = 180$ s), becomes faster with increasing temperature. Consequently, any small magnetization remaining at a temperature close to T_{irr} decays very quickly to $M = 0$. Thus T_{irr} does not depend much on the choice of time window between $t = 10^2$ and 10^4 s, as demonstrated in Fig. 10(b).

The logarithmic time dependence is characteristic of physical processes governed by thermal activation in the presence of a driving force.[1,30] In the case of critical current, the driving force is the current density J, whereas the distance from the equilibrium state provides the driving force in the magnetization measurements. In the flux creep model, the correlation time τ of the thermal fluctuations of a flux vortex is given by the Arrhenius formula of Eq. (16). The activation energy $U(M)$ at finite M is different from the equilibrium value U_0, reflecting the lowering of U for finite driving force, as $U(M) = U_0[1 - (M/M_0)]$, where M_0 represents the magnetization in the absence of thermal activation. The rate of magnetization change should then be proportional to τ^{-1} as

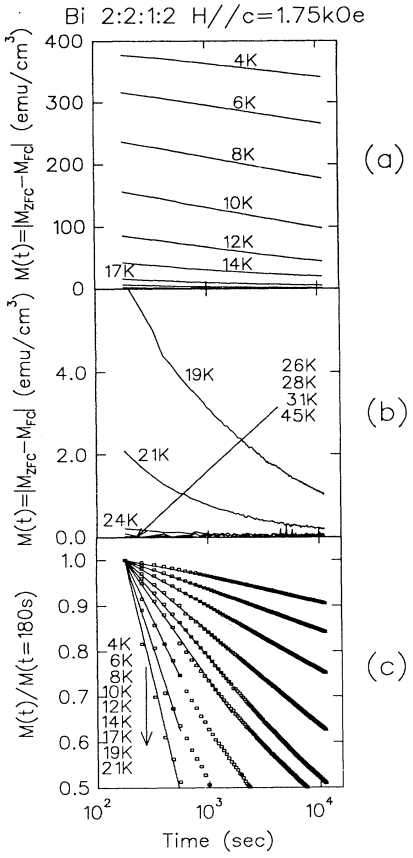

FIG. 10. (a) and (b) Magnetization decay measurements of Bi 2:2:1:2 crystals down at 4 K. At each temperature, we measured the ZFC magnetization (time dependent) and the FC magnetization (time independent). The magnetization M is the difference $|M_{\rm ZFC}-M_{\rm FC}|$. (c) Normalized magnetization by initial magnetization at $t=180$ s. The logarithmic relaxation of magnetization shown gives general support to the flux-creep model [Eq. (20)].

$$\frac{dM}{dt}\propto\tau_0^{-1}\exp[-U(M)/kT]\ . \tag{19}$$

In general, the differential equation $d\alpha/dt\propto\exp(q\alpha/kT)$ has the solution $\alpha=\text{const}-(kT/q)\ln(t)$. Therefore, Eq. (19) has an approximate solution

$$M(T,t)=M_0[1-(kT/U_0)\ln(t/t_{\rm eff})]\ , \tag{20}$$

where $t_{\rm eff}$ is an effective attempt time, which includes both τ_0 and other geometrical and field-intensity factors. This equation predicts the well-known logarithmic relaxation of the magnetization with time seen in Fig. 10(c).

It is convenient to eliminate M_0 from Eq. (20) by calculating

$$S\equiv-\frac{d\ln(M)}{d\ln(t)}=kT/[U_0-kT\ln(t/t_{\rm eff})]\ , \tag{21}$$

$$1/S=(U_0/kT)-\ln(t)+\ln(t_{\rm eff})\ . \tag{22}$$

In Fig. 11, we plotted S and $1/S$ versus $\ln(t)$ based on the magnetization measured in Bi 2:2:1:2. The solid line of Fig. 11(b) shows a parameter-independent universal slope of the logarithmic decay of $1/S$, $d(1/S)/d\ln(t)=-1$, predicted by Eq. (22). At low temperatures ($T\le 14$ K), the observed results show a decay consistent with this slope. This agreement gives a general support to the flux creep model. At temperatures closer to $T_{\rm irr}$, our results do not have enough statistical accuracy to test the consistency with Eq. (22).

In Fig. 12, we plot the temperature dependence of S at $t=180$ s measured in Bi 2:2:1:2 and Pb-Bi 2:2:1:2 crystals. At low temperatures, where U_0 is much greater than $kT\ln(t/t_{\rm eff})$, Eq. (21) predicts a linear temperature dependence for S. The data at $H_{\rm ext}=1.75$ kOe in both Bi 2:2:1:2 and Pb-Bi 2:2:1:2 exhibit this linear T dependence for $T\le 10$ K. Assuming $t_{\rm eff}\sim\tau_0=1.1\times10^{-13}$ s and fitting S to Eq. (21) in the low-temperature region, the activation energy U_0 estimated is $U_0=34$ meV for Bi 2:2:1:2 and 58 meV for Pb-Bi 2:2:1:2. Clearly the activation energy is significantly increased with Pb doping. The resistivity study of Ref. 4 found a weak dependence for the activation energy U_0 on $H_{\rm ext}$ as shown in Eq. (15). We observed a field dependence for S qualitatively consistent with that. We note that $U_0=34$ meV at $H_{\rm ext}=1.75$ kOe estimated from our magnetization study is about half of the estimate from Ref. 4. $U_0\sim65$ meV at $H_{\rm ext}=1.75$ kOe from Ref. 4 corresponds to $S\sim0.025$ at $T=10$ K in dc-susceptibility measurements. Many dc-

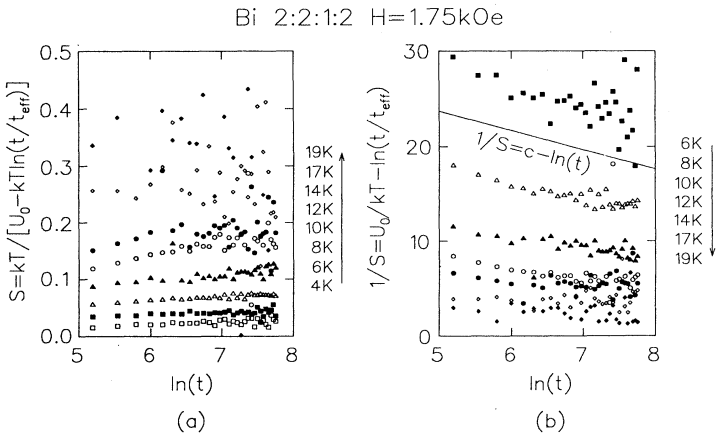

FIG. 11. (a) $S=-d\ln(M)/d\ln(t)$ and (b) $1/S$ as a function of $\ln(t)$. At low temperatures ($T\le 14$ K), $1/S$ shows a decay consistent with the parameter-independent slope $d(1/S)/d\ln(t)=-1$, as predicted by Eq. (22). The solid line in (b) represents a line of slope $d(1/S)/d\ln(t)=-1$.

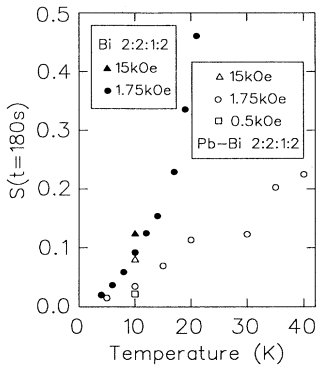

FIG. 12. Temperature dependence of $S(t=180$ s) measured in Bi 2:2:1:2 and Pb-Bi 2:2:1:2 crystals. At $H_{ext}=1.75$ kOe, $S(t=180$ s) in both crystals shows linear T dependence at $T \leq 10$ K, consistent with Eq. (21) for $U_0 \gg kT \ln(t/t_{eff})$ at low temperatures. By fitting S to Eq. (21) in the low-temperature region, we find the activation energy U_0 is significantly increased by the Pb doping (from 34 meV in Bi 2:2:1:2 to 58 meV in Pb-Bi 2:2:1:2).

susceptibility measurements in the Bi 2:2:1:2 system have reported S values of order 0.1.[30] This indicates the activation energies U_0 estimated from the dc-susceptibility measurements are usually smaller than that estimated from the resistivity measurements. The difference could reflect a possible difference in the activation energies of pinning centers between the specimens used in these two kinds of measurements, or an intrinsic difference of experimental nature.

VII. DISCUSSIONS AND CONCLUSIONS

To consider the effective time window for μSR studies of flux pinning, it is helpful to refer to the magnetization results $M(t)$ in Fig. 10. Both μSR and $M(t)$ probe how the nonequilibrium ZFC state approaches the more equilibrated FC state. The magnetization measures this phenomena in terms of the averaged flux density, whereas μSR measures it in terms of the width of the local-field distribution due to the flux lattice. Although it is not apparent how to obtain rigorous relations between the average flux density and the width, we know these two quantities are intimately correlated. Here, we adopt a working assumption that $4\pi M = 4\pi |M_{ZFC} - M_{FC}|$ roughly corresponds to the difference $\sqrt{\Delta B_{ZFC}^2 - \Delta B_{FC}^2}$ between the FC and ZFC results of width ΔB derived from the muon-spin-relaxation rate σ as $\Delta B \sim \sigma/\gamma_\mu$. Assuming that the relaxation rate σ_{FC} is about 0.5 μs^{-1} around the depinning temperature T_{irr}, and the instrumental-statistical resolution of μSR measurements is about $\Delta\sigma \sim 0.22$ μs^{-1}, we obtain the magnetic-field resolution of

$$\sqrt{\Delta B_{ZFC}^2 - \Delta B_{FC}^2} = \sqrt{\Delta\sigma_{ZFC}^2 - \Delta\sigma_{FC}^2}/\gamma_\mu \sim \sqrt{0.52^2 - 0.5^2}/\gamma_\mu = 1.4 \text{ G} .$$

Usually, each run of μSR measurements is started at $t \sim 300$ s after establishing H and T, and continues for about 1000 to 2000 s. Therefore, the irreversibility temperature T_{irr} determined by μSR should correspond to T_{irr} estimated in dc-magnetization measurements $M(t)$ with a resolution of about 1.4 G/$4\pi \sim 0.1$ emu/cm^3 in the time window $t = 10^2 - 10^3$ s according to the working assumption mentioned above. As shown in Fig. 9, the irreversibility temperatures we obtained in Bi 2:2:1:2 from μSR agree very well with those obtained by $M(t)$ with the resolution of about 0.1 emu/cm^3 and in the time window of $\sim 10^2$ s. This agreement is consistent with the above argument, and thus suggests that the effective time window of μSR for the study of flux pinning is about $10^2 - 10^3$ s.

Generally, there are two different dynamic processes probed in the study of flux pinning. The first is a transient process during approach from the nonequilibrium state to the equilibrium state under a driving force. This is measured as the difference between ZFC and FC measurements; both μSR and magnetization $M(t)$ studies derive T_{irr} based on this process. The second process is the dynamic thermal fluctuations of flux vortices at the equilibrium state, without any dc-driving force. Mechanical oscillator and ac-susceptibility measurements probe flux depinning phenomena through this second process. In Secs. V and VI, we have shown that the results of these four different measurements in Bi 2:2:1:2 agree very well and can be explained consistently within a flux-creep model, assuming roughly the same activation energies and pre-exponential factors. This feature indicates that the two processes, i.e., rearrangement of the flux vortices and their local fluctuations, likely originate from the same physical phenomena.

In our μSR studies, we obtained a higher depinning temperature T_{irr} for a given external field in Pb-Bi 2:2:1:2 than in Bi 2:2:1:2. The higher activation energy U_0 found in the SQUID magnetization study indicates that this is, at least partly, due to the deepening of the pinning potential caused by the Pb doping. The ratio of T_{irr} in Bi 2:2:1:2 and Pb-Bi 2:2:1:2 shown in Fig. 6 is about 1 to 1.8. This ratio agrees with the ratio between the activation energies of these two systems $(U_0)_{Bi}:(U_0)_{Pb\text{-}Bi} = 1:1.7$. Therefore, we conclude that a major reason for the increase of T_{irr} in Pb-Bi 2:2:1:2 is in fact the increase of U_0. It is, however, still possible that some other factors, such as the change of the density of pinning centers, play additional roles.

As shown in Fig. 7, the low-temperature relaxation rate $\sigma(T \to 0)$ in the Bi 2:2:1:2 system is about 0.5–0.7 μs^{-1} in the present single crystals. Previously we obtained $\sigma(T \to 0) = 0.8$ μs^{-1} in a thick oriented film,[10] and 1.3–1.8 μs^{-1} in unoriented sintered ceramic specimens.[10,28] A previous μSR study[32] reported about the same relaxation rate $\sigma(T \to 0) = 0.6$ μs^{-1} in single crystal specimens of Bi 2:2:1:2. This is a substantial dependence of the experimental results on sample morphology. In contrast to the Bi 2:2:1:2 system, μSR results in $YBa_2Cu_3O_7$ (Y 1:2:3) systems do not depend much on sample morphology.[33,28] The scatter in the absolute value of σ remains an unanswered mystery to μSR researchers.

There are three possible ways (a)–(c) to interpret the difference between the μSR results in single crystals and

ceramics, as follows. (a) It has been found that Bi 2:2:1:2 is susceptible to various structural defects, including modulation of the Bi-O planes, intergrowth of various phases, etc. In the process of producing the Bi 2:2:1:2 specimens, it is known[34] that oxygen diffuses much more slowly along the $\hat{c}$-axis direction than in the $\hat{a}$-$\hat{b}$ plane. It is possible that the single crystals with macroscopic size are less fully oxygenated compared to ceramic specimens having much smaller microcrystallites. In view of the phase diagram of Bi 2:2:1:2 system versus hole doping,[10] the oxygen deficiency could result in fewer hole carriers in single-crystal specimens, and consequently smaller σ. (b) The small relaxation rate in single crystals may be related to possible dynamic motional narrowing of the width of inhomogeneous local fields due to dynamic fluctuations of vortex positions. (c) The small relaxation rate in single crystals may be due to possible static rearrangement (or winding) of flux vortices, which would somehow average the randomness of local fields for a certain length scale of the "flux winding."[35] The scenarios (b) and (c) assume that ceramic specimens have more pinning centers and thus are more resistive to the dynamic or static narrowing processes.

Although we cannot provide a conclusive explanation to this mystery, we can provide some new constraints from the present study. For dynamic motional narrowing (b) to occur, it is necessary that a flux vortex moves a distance comparable to the separation between adjacent vortices within the muon lifetime $\sim 10^{-6}$ s, even at very low temperatures $T \leq 10$ K. The fluctuation time τ given by the Arrhenius formula of Eq. (16), using the activation energy and preexponential factor estimated in the present study, is much longer than the fluctuation time (microsecond) required for this motional narrowing. Therefore, we conclude that simple activation processes cannot cause the motional narrowing. One requires an entirely different process, such as quantum fluctuations of vortices, to result in dynamic narrowing.

In Ref. 32, Harshman *et al.* reported a sharp increase of the μSR relaxation rate σ in Bi 2:2:1:2 single crystals below $T \sim 25$ K, and ascribed it to the slowing down of dynamic motion of flux vortices. For reasonable values of $\tau_0 = 10^{-13}$ s and $U_0 = 700$ K, the correlation time τ given by Eq. (16) is about 0.2 s at $T = 25$ K, and of course longer than that at lower temperatures. Thus, the thermal over-barrier vortex motion is completely frozen for the time scale of μSR measurements below 25 K. On the other hand, the possible effect of quantum fluctuations, if existing, should be temperature independent. Therefore, we consider that neither the thermal nor the quantum fluctuations can explain the low-temperature increase of the relaxation rate observed in Ref. 32.

With respect to the static narrowing (c), Le[36] has performed a computer simulation for various types of flux winding. The simulation study found that the static narrowing can be expected only when the flux lines are modulated with a vertical (parallel to the flux line) modulation length scale of less than about 500 Å. Moreover, this static narrowing effect should be extremely sensitive to magnitude of applied external field, which determines inter vortex distance. As discussed in Sec. IV, the relaxation rate measured in Bi 2:2:1:2 crystals do not exhibit much field dependence. In addition, the average size of microcrystallites in ceramic specimens is more than several microns; there should be no essential difference between single crystals and ceramics for phenomena with a length scale shorter than 500 Å. These considerations lead us to believe the scenario (c) is also unlikely.

The above considerations are supported by our μSR measurements on the crushed Bi 2:2:1:2 crystals [Fig. 7(c)]. The relaxation rate $\sigma(T \rightarrow 0)$ of single-crystal specimens is increased only to $\sim 0.75\ \mu s^{-1}$ when the single crystals are crushed and pressed into a ceramic pellet. The relaxation rate is still significantly smaller than the large relaxation rate $\sigma(T \rightarrow 0) = 1.3-1.8\ \mu s^{-1}$ observed in normal ceramic specimens of Bi 2:2:1:2.[10,28] This indicates that the single-crystal specimen is different from normal ceramic specimen in the hole concentration, and that scenarios (b) and (c) are not adequate to explain the difference between the two.

A support for scenario (a) is given by the signature of static magnetic order found in zero-field μSR measurements (Fig. 8) in Bi 2:2:1:2 crystals at low temperatures $T \leq 5$ K. Since the 2:2:1:2 system with lower hole concentrations is known to exhibit static magnetic order, the appearance of static order indicates that the single-crystal sample has a substantial inhomogeneity in hole concentration. Although it is not clear if this feature can be generalized to the specimens used in previous μSR studies on 2:2:1:2 systems, the results in Fig. 8 demonstrate importance of systematically performing careful zero-field μSR measurements in the study of the penetration depth and vortex dynamics. Even after these considerations, the "mystery" of the morphological dependence of $\sigma(T \rightarrow 0)$ in the Bi 2:2:1:2 system is far from being solved. Further experimental and theoretical work will be necessary to clarify this problem unambiguously.

In a superconductor, a pinned vortex has lower free energy per unit length than a free vortex by the amount of the condensation energy per unit length ϵ_c in the flux core region

$$\epsilon_c = \frac{H_c^2}{8\pi}\pi\xi_{ab}^2 = \frac{\Phi_0^2}{64\pi^2\lambda_{ab}^2}\ , \tag{23}$$

where ξ_{ab} and λ_{ab} are the coherence length and penetration depth in the $\hat{a}$-$\hat{b}$ plane. Strong correlations between T_c and $\sigma(T \rightarrow 0) \propto 1/\lambda_{ab}^2$ were found in our previous μSR measurements in high-T_c cuprate, organic, bismuthate, Chevrel-phase, and heavy-fermion superconducting systems, which we called "exotic superconductors."[28] The values of $T_c/(1/\lambda_{ab}^2)$ in these exotic superconductors are much larger than those of conventional superconductors. The depinning temperature $T_{\rm irr}$ is determined by the competition between the thermal fluctuation and the pinning of vortices, which are characterized by temperature T and activation energy $U_0 = \epsilon_c \xi_c \propto \xi_c/\lambda_{ab}^2$, respectively. The high value of $T_c/(1/\lambda_{ab}^2)$ in the exotic superconductors makes depinning of vortices possible at the temperature $T_{\rm irr}$ measurably lower than T_c. Since ξ_c is much smaller than ξ_{ab} in very anisotropic superconductors like Bi 2:2:1:2, U_0 is much smaller in highly anisotropic su-

TABLE I. Depinning temperature.

Compound (morphology)	T_c (K)	T_{irr} (K)	T_{irr}/T_c	H (kG)	Ref.	Anisotropy	Ref.
$Bi_2Sr_2CaCu_2O_8$ (single crystal)	90	26±2	0.29±0.02	1.75	a	$\rho_c/\rho_{ab}\sim 1-4\times 10^5$ (at 100 K)	37
k-(BEDT-TTF)$_2$Cu[N(CN)$_2$]Br (single crystal)	12.3	5.0±0.5	0.41±0.04	3.0	40	$\rho_c/\rho_{ab}\sim 10^3$	42
$LiTi_2O_4$ (ceramic)	11.5	10.0±0.5	0.87±0.04	2.0	b	isotropic (cubic structure)	38
$Ba_{0.6}K_{0.4}BiO_3$ (ceramic)	24	21±1	0.88±0.04	2.0	28	isotropic (cubic structure)	
URu_2Si_2 (single crystal)	1.2	1.0±0.1	0.9±0.1	2.0	c	$\rho_c/\rho_a\sim 0.5$ (at 300 K)	39
$YBa_2Cu_3O_7$ (single crystal)	90	83±1	0.92±0.01	3.9	b	$\rho_c/\rho_{ab}\sim 1-3\times 10^2$ (at 100 K)	37
$YBa_2Cu_3O_7$ (sintered powder)	91	85±1	0.93±0.01	2.0	b		
$La_{1.85}Sr_{0.15}CuO_4$ (single crystal)	35	33±1	0.94±0.03	2.0	b	$\rho_c/\rho_{ab}\sim 4$ (at $T_c\sim 13$ K)	43
K_3C_{60} (polycrystal)	18.9	18.9±0.5	1.00±0.03	2.0	41	isotropic (fcc structure)	

[a]Present study.
[b]Unpublished.
[c]Preprint.

perconductors than in more isotropic superconductors. As a result, the flux depinning temperature of Bi 2:2:1:2 is much lower than that of $YBa_2Cu_3O_7$. Table I shows depinning temperatures for several superconductors measured by μSR. We see the tendency that the more anisotropic superconductor has a lower ratio of T_{irr}/T_c.

In summary, we have demonstrated that the flux-depinning phenomena in a high-T_c cuprate superconductor Bi 2:2:1:2 can be studied by μSR technique through comparison of relaxation rates measured in FC and ZFC procedures. The irreversibility lines obtained by μSR, time-dependent dc-magnetization, ac-susceptibility, and mechanical oscillator measurements can be explained in the framework of the flux creep model. The time window for the μSR measurements is about 10^2-10^3 s. Comparison of the μSR and magnetization results Bi 2:2:1:2 and Pb-Bi 2:2:1:2 demonstrate that the flux depinning temperature T_{irr} is significantly increased by the Pb substitution, mainly due to the increase of the activation energy U_0 in the Pb-doped system.

ACKNOWLEDGMENTS

We thank J. H. Brewer and E. M. Gyorgy for stimulating discussions, Y. L. Wang, C. J. Chen, and C. M. Lieber for teaching us to make the Bi 2:2:1:2 crystals, and C. Ballard and K. Hoyle for technical assistance. Work at Columbia is supported by NSF (Contract No. DMR-89-13784) and the David and Lucile Packard Foundation (YJU). Work at TRIUMF was supported by NSERC and NRC.

APPENDIX

1. SQUID measurements

In SQUID measurements, it is difficult to calculate how the sample geometry and the size of the detecting coils affect the SQUID response. In this appendix, we are going to illustrate several points.

Consider a simplified model of the SQUID magnetometer. We have a detecting coil with radius R in the x-y plane and a dipole moment $\mathbf{m}=(0,0,m)$ is moved to $(\rho,0,z)$ from infinity. The response of the system is proportional to the magnetic flux $\phi=\oint\mathbf{B}\cdot d\mathbf{s}$ through the detecting coil.

$$\phi=-\int_R^\infty\int_0^{2\pi}B_z r\,dr\,d\theta \tag{A1}$$

$$=-\int_R^\infty\int_0^{2\pi}\left[\frac{3mz^2}{r_1^5}-\frac{m}{r_1^3}\right]r\,dr\,d\theta\ , \tag{A2}$$

where r_1 is distance between the dipolar moment and an arbitrary point $(r\cos\theta,\ r\sin\theta,\ 0)$ in the x-y plane,

$$r_1^2=(\rho-r\cos\theta)^2+(r\sin\theta)^2+z^2\ . \tag{A3}$$

In the expression for ϕ, we have used the fact that the total magnetic flux through the x-y plane is zero.

When $\rho=0$, that is, the dipolar moment is on the z axis,

$$\phi=\frac{2\pi m}{R}\frac{1}{(1+z^2/R^2)^{3/2}}\ . \tag{A4}$$

When $\rho\neq 0$, by expanding B_z in series of z/r and ρ/r, ϕ can be calculated to second order in z/r and ρ/r,

$$\phi=\frac{2\pi m}{R}\left[1+\frac{3}{4}\frac{\rho^2-2z^2}{R^2}\right]\ . \tag{A5}$$

Therefore, if a small sample with a homogeneous magnetization $M=m/V$ is put at the center of the detecting coil, we have

$$\phi=\frac{2\pi MV}{R}\left[1+\frac{3}{4}\frac{\bar{\rho}^2-2\bar{z}^2}{R^2}\right]\ . \tag{A6}$$

Equation (A6) shows that, with a fixed total moment m, a disk-shaped sample produces more magnetic flux through the detecting coil than a rod-shaped sample does. For a practical SQUID magnetometer, a point-dipole-moment is assumed to derive magnetization from response. Therefore, the measured magnetization M_{obs} can be expressed as

$$M_{obs}=\frac{R}{2\pi V}\phi=\frac{R}{2\pi V}\oint_{coil}(\mathbf{B}-\mathbf{H}_{ext})\cdot d\mathbf{s}\ . \tag{A7}$$

Equation (A6) indicates that the measured magnetization M_{obs} differs from the real magnetization M by

$$\frac{M_{\rm obs}}{M}=1+\frac{3}{4}\frac{\bar{\rho}^2-2\bar{z}^2}{R^2} . \quad \text{(A8)}$$

This shows that $M_{\rm obs}=M$ holds when $\bar{\rho}^2 \ll R^2$ and $\bar{z}^2 \ll R^2$.

For a small cylinder of diameter D and length L with homogeneous magnetization M, we have

$$\frac{M_{\rm obs}}{M}=1+\frac{3}{8}\left[\frac{D}{2R}\right]^2-\frac{1}{2}\left[\frac{L}{2R}\right]^2 . \quad \text{(A9)}$$

Applying this equation to the SQUID magnetometer used in our measurements, with $R=10$ mm and $D=5$ mm, we find that $M_{\rm obs}/M=1.02$ when $L=1$ mm, and $M_{\rm obs}/M=0.90$ when $L=10$ mm. Since our $Bi_2Sr_2CaCu_2O_8$ and $Pb_{0.7}Bi_{1.3}Sr_2CaCu_2O_8$ crystals all have dimensions $D \le 5$ mm and $L \le 0.2$ mm, $M_{\rm obs}=M$ holds for our measurements with an error less than 3%.

2. Demagnetizing effect

The above discussion shows that the relation between $M_{\rm obs}$ and M relies on both specimen geometry and size of detecting coils. On the other hand, M is related to the specimen geometry as following. In any magnetic system with uniform response M to an applied field $H_{\rm ext}$, we always have

$$B=H+4\pi M , \quad \text{(A10)}$$

$$H=H_{\rm ext}-4\pi N M , \quad \text{(A11)}$$

where N is the so-called demagnetizing factor. A susceptibility χ defines the relation between M and H as $4\pi M=\chi H$; we then obtain

$$\frac{4\pi M}{H_{\rm ext}}=\frac{\chi}{1+N\chi} . \quad \text{(A12)}$$

Equation (A12) indicates that the demagnetizing effect (or "shape effect") becomes much less important for a weak magnetic specimen with $|\chi| \ll 1$ than for a superconductor in the Meissner state with $\chi=-1$. Except for a specimen of long rod or ellipsoid of rotation, M and N are generally not homogeneous inside the specimen. Nevertheless, Eq. (A12) still holds for averaged M and N, and the demagnetizing effect is negligible for a magnetic system with $|\chi| \ll 1$. The weak magnetism $|\chi| \ll 1$ can be realized in a paramagnetic specimen, or by cooling a type-II superconductor in a field $H_{\rm ext} \gg H_{c1}$ (field-cooling measurements). When $|\chi| \ll 1$, specimens of arbitrary shape have the same magnetization $4\pi M=\chi H_{\rm ext}$.

When a magnetic field $H_{\rm ext} \le (1-N)H_{c1}$ is applied to a type-II superconductor with a demagnetizing factor N, the superconductor is in the Meissner state with $B=0$. A Meissner state can be experimentally better approximated by a zero-field-cooling (ZFC) process than a field-cooling (FC) process due to flux pinning. In the Meissner state, the fictitious field $H=H_{\rm ext}/(1-N)$ inside the superconductor is quite different from the external field $H_{\rm ext}$ for a large demagnetizing factor N.

In ZFC measurements with $H_{\rm ext} \ge (1-N)H_{c1}$, magnetization of the superconductor can be much larger than FC magnetization due to flux pinning, resulting in a large susceptibility $|\chi|$. We have noted that, for a fixed magnetic flux density B inside the superconductor, $4\pi M/H_{\rm ext}$ could be large if the demagnetizing factor N is close to 1. Following Eq. (A12), we obtain

$$\frac{4\pi M}{H_{\rm ext}}=\frac{\chi}{1+N\chi}=\frac{B}{H_{\rm ext}}-\frac{1}{1+N\chi} . \quad \text{(A13)}$$

In the case of $B/H_{\rm ext}=5/7$ (most of the flux lines still penetrate into the superconductor) and $N=0.9$, we have $\chi=-0.8$, and $-4\pi M/H_{\rm ext}=20/7$, which is significantly larger than 1.

Now we consider the validity of Eq. (2) in Sec. II, which was derived for an infinitely long, rectangular sample with the assumption $H_{\rm ext} \gg H_{c1}$ (ZFC measurements). The assumption $H_{\rm ext} \gg H_{c1}$ also guarantees that the system is weakly magnetized, that is, $|\chi| \ll 1$. Since the demagnetizing effect is negligible in this case, Eq. (2) can be used in measurements of a thin plate without modification. For small $H_{\rm ext}$, more careful calculation with the critical state model for an infinitely long sample shows that Eq. (2) provides an underestimation of J_c.[44] In the case of thin-plate samples, the demagnetizing effect becomes important.

In our measurements of the Bi 2:2:1:2 and Pb-Bi 2:2:1:2 crystals, we obtain $-4\pi M/H_{\rm ext} \sim 0.2$ for Bi 2:2:1:2 and ~ 2 for Pb-Bi 2:2:1:2 at $H_{\rm ext}=10$ kOe. This indicates that the Bi 2:2:1:2 crystal is indeed weakly magnetized, but the Pb-Bi 2:2:1:2 crystal not. Therefore, Eq. (2) can be used to estimate J_c in the Bi 2:2:1:2 crystal, but it should be modified properly to obtain J_c in the Pb-Bi 2:2:1:2 crystal. Unfortunately, the modification of Eq. (2) for a specimen of demagnetizing factor N is quite difficult. Instead, in Sec. II, we found a way to compare J_c between two specimens of the same shape by using the ratio of the magnetizations at $H_{\rm ext}=0$.

[1] A. P. Malozemoff, in *Physical Properties of High Temperature Superconductors I*, edited by D. M. Ginsberg (World Scientific, Singapore, 1989), Chap. 3; Y. B. Kim and M. J. Stephen, in *Superconductivity*, edited by R. D. Parks (Marcel Dekker, New York, 1969), Chap. 19.

[2] P. W. Anderson, Phys. Rev. Lett. **9**, 309 (1962); P. W. Anderson and Y. B. Kim, Rev. Mod. Phys. **36**, 39 (1964).

[3] M. V. Feigel'man, V. B. Geshkenbein, and A. I. Larkin, Physica C **167**, 177 (1990); A. Houghton, R. A. Pelcovits, and A. Sudbø, Phys. Rev. B **40**, 6763 (1989); D. S. Fisher, *ibid.* **22**, 1190 (1980).

[4] T. T. M. Palstra, B. Batlogg, L. F. Schneemeyer, and J. V. Waszczak, Phys. Rev. Lett. **61**, 1662 (1988).

[5] P. L. Gammel, L. F. Schneemeyer, J. V. Waszczak, and D. J. Bishop, Phys. Rev. Lett. **61**, 1666 (1988).

[6] J. T. Kucera, D. G. Steel, D. W. Face, J. M. Graybeal, T. P. Orlando, and D. A. Rudman, Physica C **162-164**, 671 (1989), and references therein.

[7] For examples of applications of μSR techniques, see A. Schenck, *Muon Spin Rotation Spectroscopy* (Hilger, Bristol,

1985); the proceedings of the five previous international conferences in this field: Hyperfine Interact. **6** (1979); **8** (1981); **17-19** (1984); **31** (1986); and **63-65** (1990).

[8]For μSR studies in high-T_c systems, see, for example, H. Keller, IBM J. Res. Develop. **33**, 314 (1989); Y. J. Uemura *et al.*, Physica C **162-164**, 857 (1989), and references therein.

[9]B. Pümpin *et al.*, Z. Phys. B **72**, 175 (1988).

[10]B. J. Sternlieb *et al.*, Physica C **162-164**, 679 (1989).

[11]P. Zimmermann, H. Keller, W. Kündig, P. Pümpin, I. M. Savić, J. W. Schneider, and H. Simmler, Hyperfine Interact. **63**, 33 (1990).

[12]A. Umezawa *et al.*, Phys. Rev. B **36**, 7151 (1987).

[13]B. Roas *et al.*, Appl. Phys. Lett. **54**, 1051 (1989).

[14]L. E. Niou *et al.*, Appl. Phys. Lett. **55**, 1575 (1989).

[15]D. Shi *et al.*, Phys. Rev. B **40**, 5255 (1989); S. X. Dou *et al.*, Supercond. Sci. Technol. **2**, 308 (1989).

[16]Yue Li Wang, Xian Liang Wu, Chia-Chun Chen, and Charles M. Lieber, Proc. Nat. Acad. Sci. USA **87**, 7058 (1990).

[17]L. F. Schneemeyer *et al.*, Nature (London) **332**, 422 (1988).

[18]A. Wiśniewski *et al.*, Physica C **170**, 333 (1990).

[19]J. D. Livingston and W. DeSorbo, in *Superconductivity,* edited by R. D. Parks (Marcel Dekker, New York, 1969), Chap. 21; J. A. Cape and J. M. Zimmerman, Phys. Rev. **153**, 416 (1967); J. P. Rice, D. M. Ginsberg, M. W. Rabin, K. G. Vandervoort, G. W. Crabtree, and H. Claus, Phys. Rev. B **41**, 6532 (1990).

[20]L. Krusin-Elbaum, A. P. Malozemoff, Y. Yeshurun, D. C. Cronemeyer, and F. Holtzberg, Physica C **153-155**, 1469 (1988).

[21]C. P. Bean, Phys. Rev. Lett. **8**, 250 (1962); M. Tinkham, *Introduction to Superconductivity* (McGraw-Hill, New York, 1985) (reprint edition), p. 171.

[22]R. B. van Dover *et al.*, Nature (London) **342**, 55 (1989); E. M. Gyorgy, R. B. van Dover, K. A. Jackson, L. F. Schneemeyer, and J. V. Waszczak, Appl. Phys. Lett. **55**, 283 (1989); C. P. Bean, Rev. Mod. Phys. **36**, 31 (1964).

[23]A. Abrikosov, Zh. Eksp. Teor. Fiz. **32**, 1442 (1957) [Sov. Phys. JETP **5**, 1174 (1957)].

[24]A. G. Redfield, Phys. Rev. **162**, 367 (1967).

[25]P. Pincus, A. C. Gossard, V. Jaccarino, and J. H. Wernick, Phys. Lett. **13**, 21 (1964).

[26]E. H. Brandt, Phys. Rev. B **27**, 2349 (1988).

[27]Y. J. Uemura *et al.*, Phys. Rev. Lett. **59**, 1045 (1987); J. H. Brewer *et al.*, Phys. Rev. Lett. **60**, 1073 (1988); W. J. Kossler *et al.*, Phys. Rev. B **35**, 7133 (1987).

[28]Y. J. Uemura *et al.*, Phys. Rev. Lett. **62**, 2317 (1989); **66**, 2665 (1991).

[29]B. J. Sternlieb *et al.*, Phys. Rev. B **40**, 11 320 (1989).

[30]A. P. Malozemoff, Physica C **185-189**, 264 (1991); P. Svedlindh *et al.*, Physica C **176**, 336 (1991).

[31]P. H. Kes and C. J. van der Beek, Physica B **169**, 80 (1991).

[32]D. R. Harshman *et al.*, Phys. Rev. Lett. **67**, 3152 (1991).

[33]Y. J. Uemura *et al.*, Phys. Rev. B **38**, 909 (1988); W. Barford and J. M. F. Gunn, Physica C **156**, 515 (1988); C. L. Seaman *et al.*, Phys. Rev. B **42**, 6801 (1990).

[34]M. Runde *et al.*, Phys. Rev. B **45**, 7375 (1992-I); S. J. Rothman, J. L. Routbort, U. Welp, and J. E. Baker, *ibid.* **44**, 2326 (1991-I); S. J. Rothman, J. L. Routbort, and J. E. Baker, *ibid.* **40**, 8852 (1989).

[35]E. H. Brandt, Phys. Rev. Lett. **66**, 3213 (1991); E. H. Brandt, Phys. Rev. Lett. **67**, 2219 (1991).

[36]In the simulation, Le assumed a Gaussian deviation of vortices from their equilibrium positions and a correlation length τ along the $\hat{c}$-axis direction. When $\lambda/a \sim 3$ (a is the distance between two adjacent vortices), one expects $\sigma_z/\sigma_{\text{perfect}} < 1.0$ (motional narrowing) only for $\tau/a < 1.0$.

[37]B. Batlogg, in *High Temperature Superconductivity,* Proceedings of the Los Alamos Symposium 1989, edited by K. S. Bedell, D. Coffey, D. E. Meltzer, D. Pines, and J. R. Schrieffer (Addison-Wesley, Reading, Mass., 1990), Chap. 2.

[38]M. R. Harrison, P. P. Edwards, and J. B. Goodenough, Philos. Mag. B **52**, 679 (1985).

[39]T. T. M. Palstra, A. A. Menovsky, and J. A. Mydosh, Phys. Rev. B **33**, 6527 (1986).

[40]L. P. Le *et al.*, Phys. Rev. Lett. **68**, 1923 (1992).

[41]Y. J. Uemura *et al.*, Nature (London) **352**, 605 (1991).

[42]Jack. M. Williams *et al.*, Science **252**, 1501 (1991).

[43]T. Ito, H. Takagi, S. Ishibashi, T. Ido, and S. Uchida, Nature (London) **350**, 596 (1991).

[44]P. Chaddah, K. V. Bhagwat, and G. Ravikumar, Physica C **159**, 570 (1989).